Symkom 2014 **Open Access**

David Garcia*, Matthew Stickland, and Grzegorz Liśkiewicz

Dynamical system analysis of unstable flow phenomena in centrifugal blower

DOI 10.1515/eng-2015-0036
Received Jan 20, 2015; accepted May 26, 2015

Abstract: Methods of dynamical system analysis were employed to analyze unsteady phenomena in a centrifugal blower. Pressure signals gathered at different control points were decomposed into their Principal Components (PCs) by means of Singular Spectrum Analysis (SSA). Certain number of PCs was considered in the analysis based on their statistical correlation. Projection of the original signal onto its PCs allowed to draw the phase trajectory that clearly separated non-stable blower working conditions from its regular operation.

Keywords: Singular Spectrum Analysis; Nonlinear dynamics; Statistical pattern recognition; compressor; surge

1 Introduction

1.1 Unstable phenomena in centrifugal compressors

Compressing units (compressors, blowers and fans) are known to have certain limitations in their operational range. At low mass flow rate the machine is prone to enter unstable working conditions, which may lead to severe damage. Therefore, much attention has been devoted to the development of mathematical description of compressor instabilities in the literature. The most dangerous flow instability was named as "surge" [1]. The first, and to date most cited attempt of surge modelling was conducted by Greitzer [2]. In his work, a four-dimensional surge model was developed and later confirmed experimentally [3]. Although the Greitzer model was originally created for axial units, it has been found that the two-dimensional version of this model can be successfully applied to describe the surge phenomenon in centrifugal units [4].

Another remarkable unstable phenomenon is the rotating stall that was first modelled by Moore and Greitzer [5, 6]. This model was further developed by many researchers, including Gravdahl and Egeland [7] and Ishii and Kashiwabara [8]. In the case of centrifugal units, some models have been proposed for particular locations of the rotating stall. *Vaneless diffuser rotating stall* (VDRS) was modelled by Jansen [9]. The model was subsequently improved by Senoo et al. [10], Abdelhamid and Bertrand [11], and Fink and van den Braembussche [12]. Abdelhamid and Bertrand revealed also that in certain conditions it is possible to initiate the rotating stall that is incepted in the rotor outlet region that propagates towards the rotor. Such a flow structure is usually referred to as *abrupt impeller rotating stall* (AIRS). Some researchers, including Lenneman and Howard [13], have reported that the rotating stall can be also gradually initiated at the inducer, which is usually associated with the term *progressive impeller rotating stall* (PIRS). Upstream of the impeller some researchers have reported presence of recirculating flow, usually referred to as *inlet recirculation* (IR) [14, 15].

1.2 Dynamical analysis of compressing units

Apart from the fact that the most crucial unstable flow structures present in centrifugal units have been named and identified, the overall process of entering unstable regime is still too complex to be fully predicted and modelled. On the other hand, understanding of this mechanism is crucial for efficient machine protection. We wish to be able to identify the moment at which the machine is on the verge of unstable operation in order to avoid entering this dangerous operational range. This need can be addressed by further development of analytical models describing particular flow structures such as the surge, VDRS, AIRS, PIRS, IR and others.

Another approach was suggested by Packard et al. [16] and Takens [17]. It includes analysis of the time series of parameters measured at the experimental stand. The

***Corresponding Author: David Garcia:** Mechanical and Aerospace Engineering, University of Strathclyde, 75 Montrose Street Glasgow G1 1XJ; Email: david.garcia@strath.ac.uk
Matthew Stickland: Mechanical and Aerospace Engineering, University of Strathclyde, 75 Montrose Street Glasgow G1 1XJ
Grzegorz Liśkiewicz: Institute of Turbomachinery, Łodz University of Technology, 90–924 Łódź, ul. Wólczańska 219/223

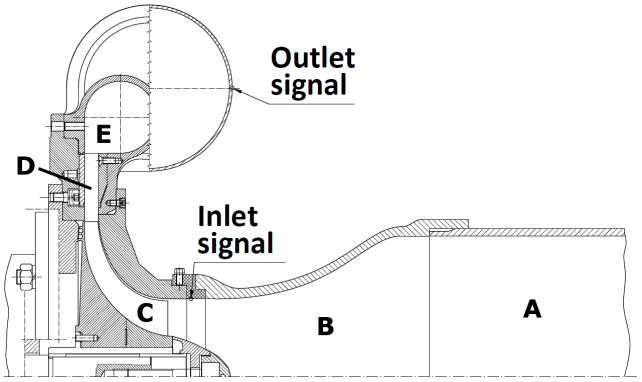

Figure 1: Cross section of the experimental rig used in this study

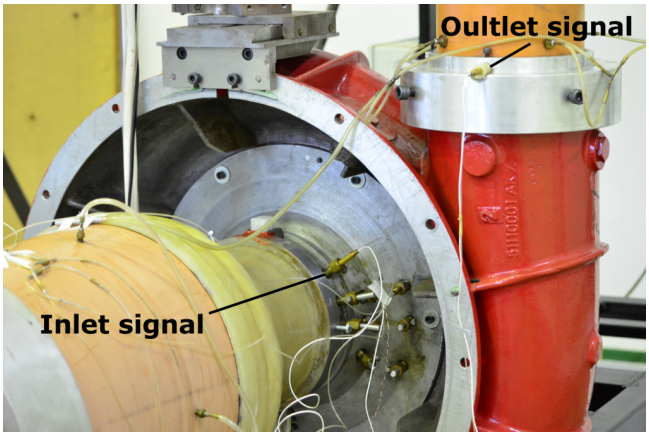

Figure 2: Experimental rig used in this study

signal is presented in the phase space constructed from derivatives [16] or by the method of delays [17]. Time series is plotted in the phase space, which reveals cyclic behavior characteristic for particular state of the machine. For example, the phase portrait of the rotating stall was observed by Palomba and Breugelmans [18] and Palomba et al. [19]. Hagino et al. [20] confirmed that this method can be used to predict the surge inception.

Aforementioned methods are strongly affected by signal noise, which have made reading of the phase portrait much disturbed. This situation can be improved by application of the singular value decomposition technique (SVD) proposed by Broomhead and King [21]. This method allows to reduce the dimension of the problem.

Komatsubara and Mizuki [22] applied it to the time series registered in the centrifugal compressor and reconstructed the phase portrait that preserved the nature of the surge cycle. Gu et al. [23] studied two centrifugal compressors to observe how the phase portrait evolved at inception of the unstable phenomena.

1.3 Aim of study

The aim of this study is to provide phase portrait reconstruction of the pressure signals gathered at different points close to the surge onset. The phase portrait reconstruction is done with the method known as the principal component analysis (PCA). The intention of such a work is allow to confirm or deny the applicability of PCA for instability detection and dynamical analysis of the signals.

2 Experimental Procedure

2.1 Experimental rig

A single stage centrifugal blower was the object of investigation. Figure 1 presents the cross-section of the blower. The flow entered the rig through the inlet pipe (A) of diameter D_{in} = 300 mm. Then, it was accelerated in the Witoszynski nozzle [24] (B) and directed towards the impeller (C). The rotor inlet diameter at the hub equaled D_{1hub} = 86.3 mm, and the inlet span equaled b_1 = 38.9 mm. At the outlet, the diameter and the span equaled D_2 = 330 mm and b_2 = 14.5 mm, respectively. The gap between the blade tip and the shroud was maintained constant at δ = 0.8 mm along the entire blade. Downstream of the rotor, air entered the vaneless diffuser (D). The diffuser outlet diameter was equal to D_3 = 476 mm. Afterwards, flow entered the circular volute (E). The volute radius was gradually increasing streamwise from the volute tongue gap of 5 mm towards the outlet pipe of diameter D_{out} = 150 mm. A throttling valve was mounted at the end of the outlet pipe. The rotor was driven by an asynchronous AC motor. The blower was designed to operate at ambient inlet conditions. The design point was attained at , $\dot{m}$ = 0.8 $\frac{\text{kg}}{\text{s}}$ and pressure ratio PR = 1.12. However, in this study, in order to avoid a risk of the impeller damage at surge, the unit was run with slightly lower rotational speed of f_{rot} = 100 Hz, with nominal flow rate of $\dot{m}_n$ = 0.75 $\frac{\text{kg}}{\text{s}}$ and pressure ratio of PR = 1.08. Rotational speed yielded the impeller tip speed equal to u_{tip} = 103 $\frac{\text{m}}{\text{s}}$. The impeller had z = 23 blades.

The test stand was equipped with 2 dynamic subminiature Kulite transducers connected to an Iotech Wavebook 516/E data acquisition system. Transducers were mounted flush to the walls to measure the static pressure at the rotor inlet and at the volute outlet. Gauge positions are presented in Figure 1. Figure 2 presents the overview of the test stand with indication of positions of the gauges.

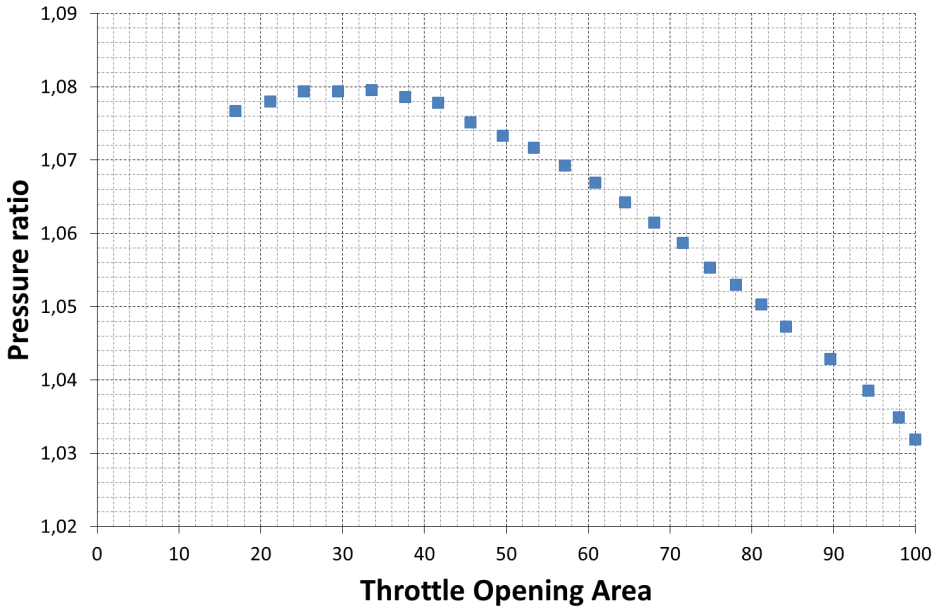

Figure 3: Blower performance curve relative to the TOA parameter

Position of the throttling valve was described by the dimensionless throttle opening area parameter referred to as TOA. TOA = 100% corresponds to fully opened valve, while TOA = 0% corresponds to fully closed valve. Each measurement contained 2^{21} samples gathered with the frequency of 100 kHz.

2.2 Singular Spectrum Analysis Technique

The methodology used here is based on Principal Component Analysis (PCA), which is a statistical procedure that uses an orthogonal transformation to convert a set of multivariate observations into a set of linearly correlated variables. However, PCA generally assumes that the data components are independent, but in the case of time series, the values are generally non-independent, and thus an extension of PCA called Singular Spectrum Analysis (SSA) provides a better alternative [25, 26]. SSA is PCA applied to lag versions of a single time series variable. It follows the following four steps [27]:

Data collection

The variables measured, in this particular case the pressure, are arranged into N-element vectors as $x^i = (x_1^i, x_2^i, \ldots, x_j^i, \ldots, x_N^i)'$ where $i = 1,2,\ldots, M$ and $j = 1,2,\ldots, N$.

Embedding

Given a window with length $W(1 < W \leq \frac{N}{2})$ the W-time lagged vectors arranged in columns are used to define the trajectory matrix $\tilde{X}$. These vectors are padded with zeros to keep the same vector length as is shown in Equation 1. The embedding matrix $\tilde{X}$ is the representation of the system in a succession of overlapping vectors of the time series by W-points.

$$\tilde{X} = \begin{pmatrix} x_1 & x_2 & x_3 & \ldots & x_w & \ldots & x_W \\ x_2 & x_3 & x_4 & \ldots & x_{w+1} & \ldots & x_{W+1} \\ x_3 & x_4 & x_5 & \ldots & x_{w+2} & \ldots & x_{W+2} \\ x_4 & x_5 & x_6 & \ldots & x_{w+3} & \ldots & \vdots \\ x_5 & x_6 & \vdots & \ldots & \vdots & \ldots & x_N \\ x_6 & \vdots & \vdots & \ldots & x_N & \ldots & 0 \\ \vdots & \vdots & x_N & \ldots & 0 & \ldots & 0 \\ \vdots & x_N & 0 & \ldots & 0 \ldots & 0 & \\ x_N & 0 & 0 & \ldots & 0 & \ldots & 0 \end{pmatrix} \quad (1)$$

Decomposition

The Empirical Orthogonal Functions (EOFs), which represent the principal directions of the system, are calculated by the decomposition into eigenvalues of $\frac{\tilde{X}'\tilde{X}}{N}$, which is equivalent to a Singular Value Decomposition (SVD). The decomposition into eigenvalues yields k-eigenvalues and

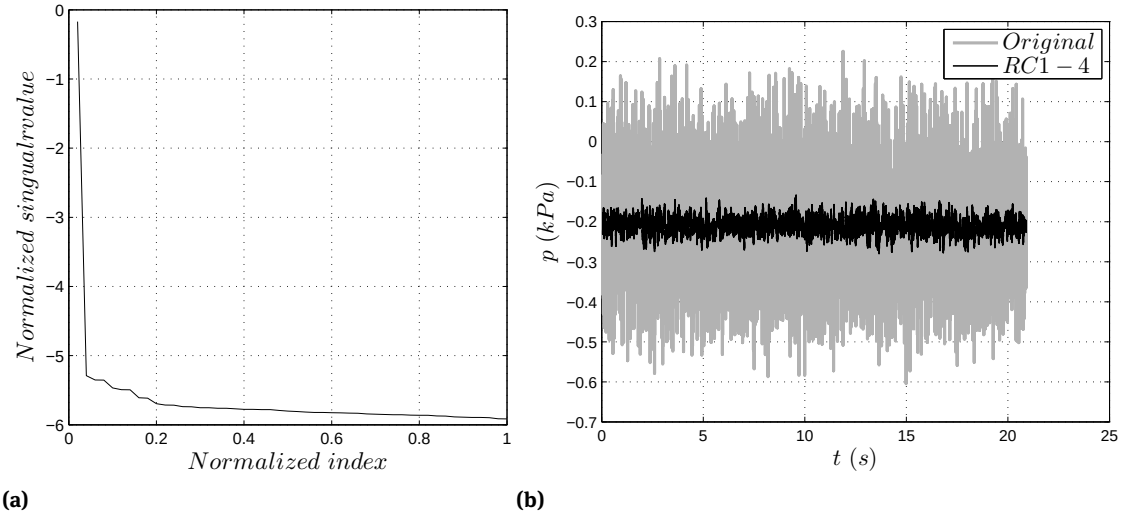

Figure 4: a) Singular value spectra and b) Source signal and sum of its three first principal components at stable working conditions (TOA = 30%) at the blower inlet

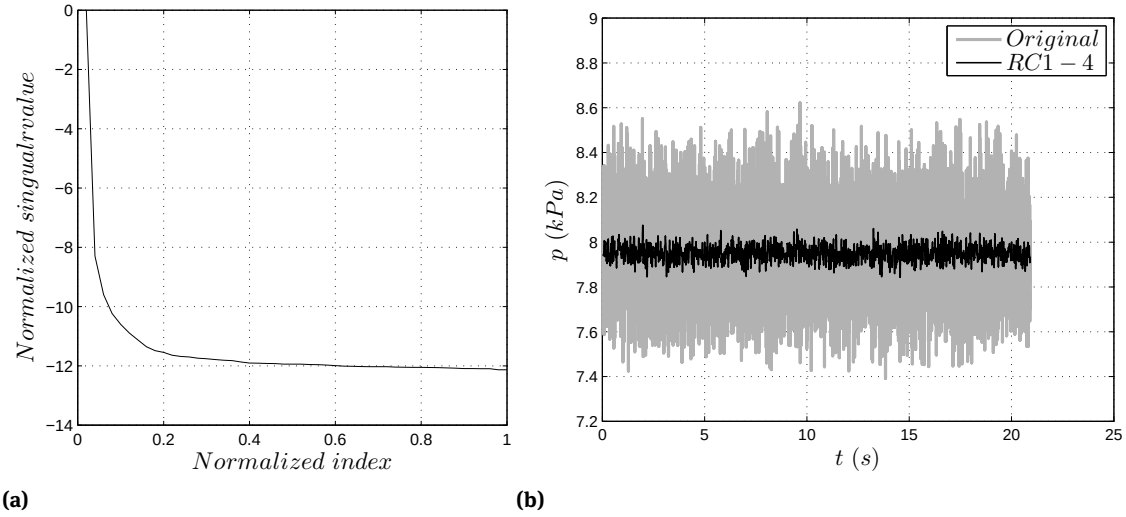

Figure 5: a) Singular value spectra and b) Source signal and sum of its three first principal components at stable working conditions (TOA = 30%) at the blower outlet

k-eigenvectors that define the orthonormal basis of the decomposition of $\tilde{X}$;

Reconstruction

The EOFs represent the data as a decomposition of the orthogonal basis functions with a certain percentage of variance of the original signal corresponding to each EOF. The data in $\tilde{X}$ is projected onto the subspace $\mathcal{L}^k$ built by the EOFs and the corresponding Principal Components (PC) [28].

2.3 Phase Portrait Reconstruction

The decomposition into a certain number of PCs of the source signal provides the distribution of the auto-correlated variance among these components.

Projecting the measured data $\tilde{X}$ onto the EOFs matrix yields the corresponding PC matrix A, which contains the

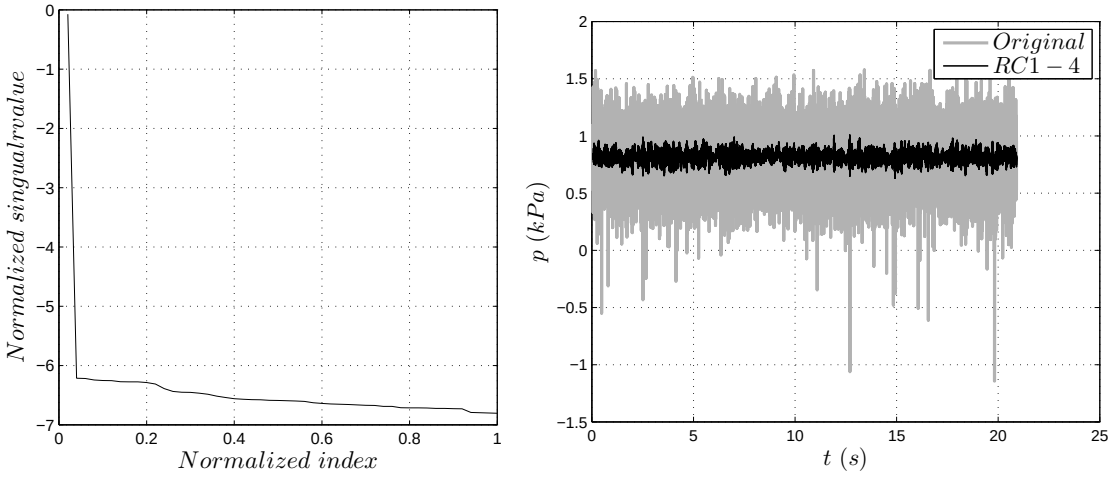

Figure 6: a) Singular value spectra and b) Source signal and sum of its three first principal components at inlet recirculation (TOA = 20%) at the blower inlet

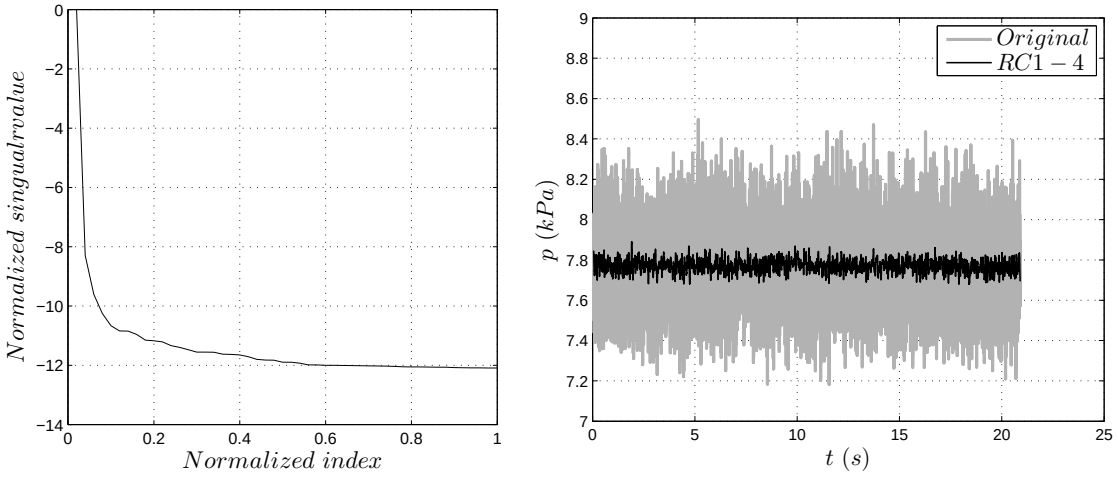

Figure 7: a) Singular value spectra and b) Source signal and sum of its three first principal components at inlet recirculation (TOA = 20%) at the blower outlet

variance information distributed among these PCs as is shown in Equation 2.

$$\tilde{A} = \tilde{X}E_X \tag{2}$$

where E_X are the eigenvectors allocated in columns.

It is now required to reconstruct the original signal data in terms of the new PCs. For this purpose, a matrix which projects the PC's back onto the new subspace is created. The Reconstructed Components (RCs) are obtained according to Equation 3. For a given set of k indices corresponding to the set of Principal Components, the RCs are obtained by projecting the corresponding PCs onto the EOFs.

$$R_n^k = \frac{1}{W}\sum_{w=1}^{W} A_{n-w}^k E_w^k \tag{3}$$

where k–eigenvectors give the k^{th} RC at n–time between $n = 1 \ldots N$, which was embedded in w lagged vectors with the maximum W length.

The variance is distributed into the RCs in a decreasing order from the first components until the last ones.

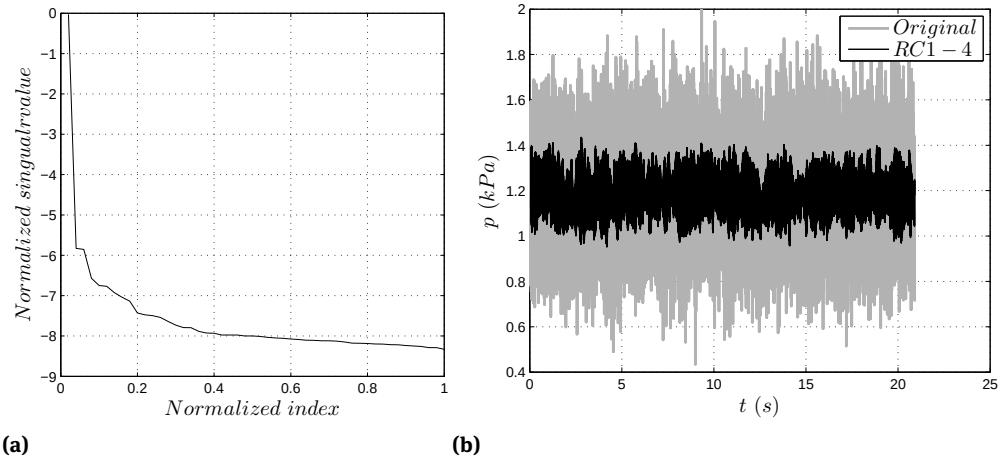

Figure 8: a) Singular value spectra and b) Source signal and sum of its three first principal components at transient phase (TOA=10%) at the blower inlet

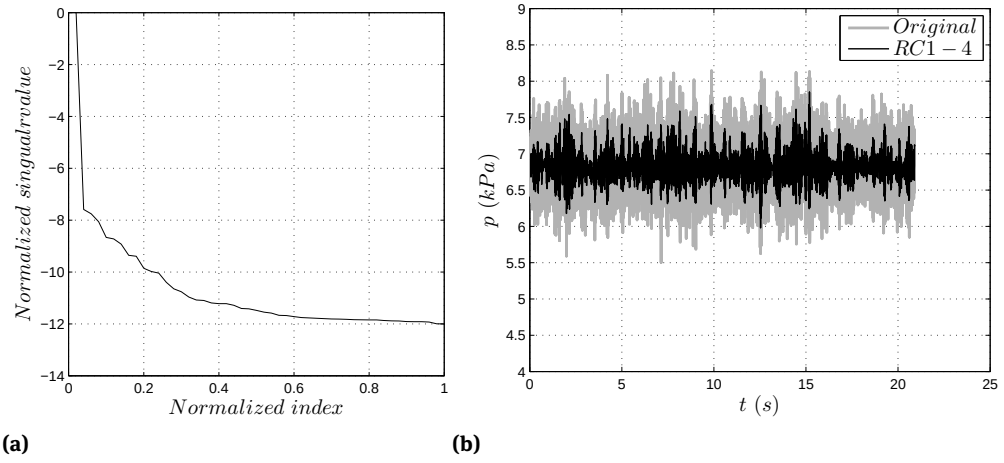

Figure 9: a) Singular value spectra and b) Source signal and sum of its three first principal components at transient phase (TOA=10%) at the blower outlet

Therefore, the first RCs contain much more descriptive information of the dynamical system than next ones. By the use of a certain number of RCs, an approximated reconstructed source signal is developed. To analyze the information contained in the RCs and hence find distinguishable information about the different dynamical systems a phase portrait was developed. The SSA methodology was applied for the source signals obtained by different Throttle Opening Area (TOA) for 5%, 10%, 20% and 30%, and the three first RCs of each signal, were used to construct the phase portraits. The singular value approach generates averages of data within the window length. Therefore, the phase portrait can improve their quality due to the RCs considered, and are above the noise floor [21]. The phase portraits constructed by the RCs can be compared with the phase portraits elaborated by the derivations of the source signals. The results obtained by the RCs plots are expected to have a better quality due to their noise reduction.

3 Results

3.1 Machine performance curve

The machine performance curve is presented in Figure 3. For convenience it is presented in dimensionless space with the pressure ratio on the vertical axis and the TOA

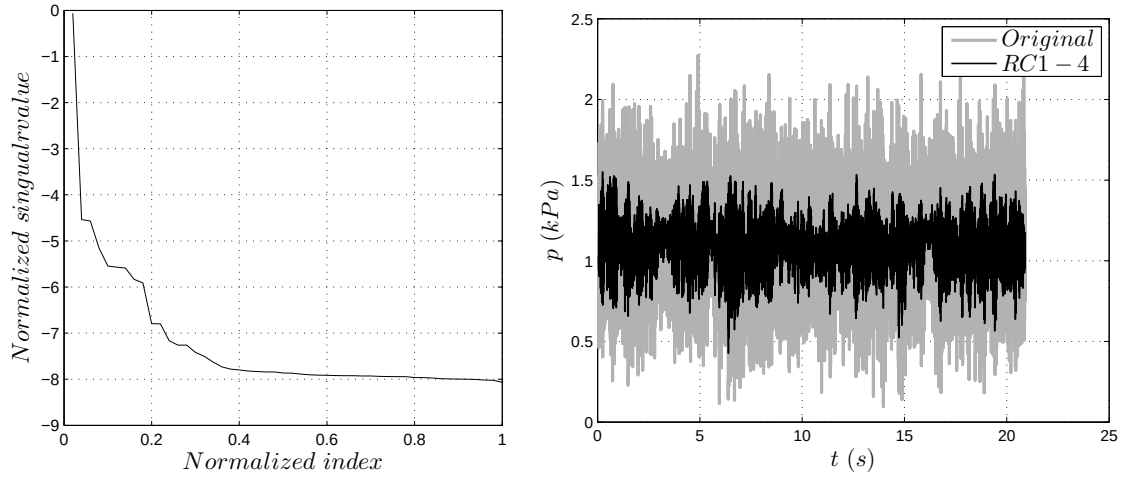

Figure 10: a) Singular value spectra and b) Source signal and sum of its three first principal components at deep surge (TOA=5%) at the blower inlet

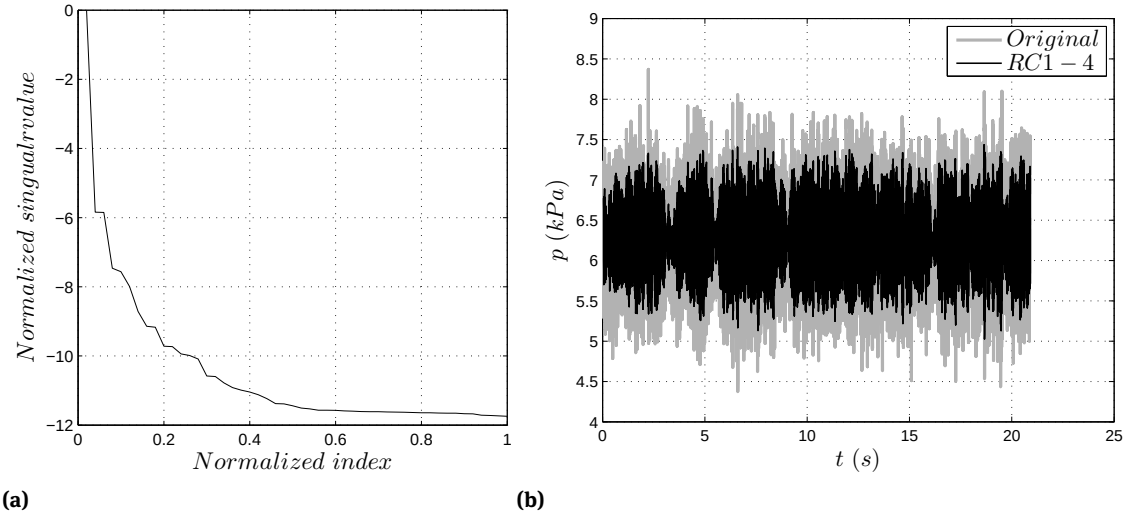

Figure 11: Source signal and sum of its three first principal components at deep surge (TOA=5%) at the blower outlet

parameter on the horizontal one. One can observe the position of the four key points chosen for this analysis: TOA = 30%, which corresponds to the highest pressure ratio, 20%, 10%, and 5%.

For each of these valve positions the signal was decomposed into components by means of the PCA with window length $W = 50$. Such a length was chosen according to the method presented by Komatsubara and Mizuki [22]. It corresponded to frequency close to the blade passing frequency, over which there was no significant energy in the Fourier spectrum.

3.2 Decomposition of signal into principal components

Figures 4 – 11 present the results of signal decomposition onto principal components. Each figure consists of two subplots. Subplot (a) presents the normalized singular value versus normalized index, which are calculated following Equation 4, where σ_i is the singular value and i are the singular value index. The number of points that define the scree diagram in Figures 4(a) to 11(a) depends on the window length. In this particular case the number

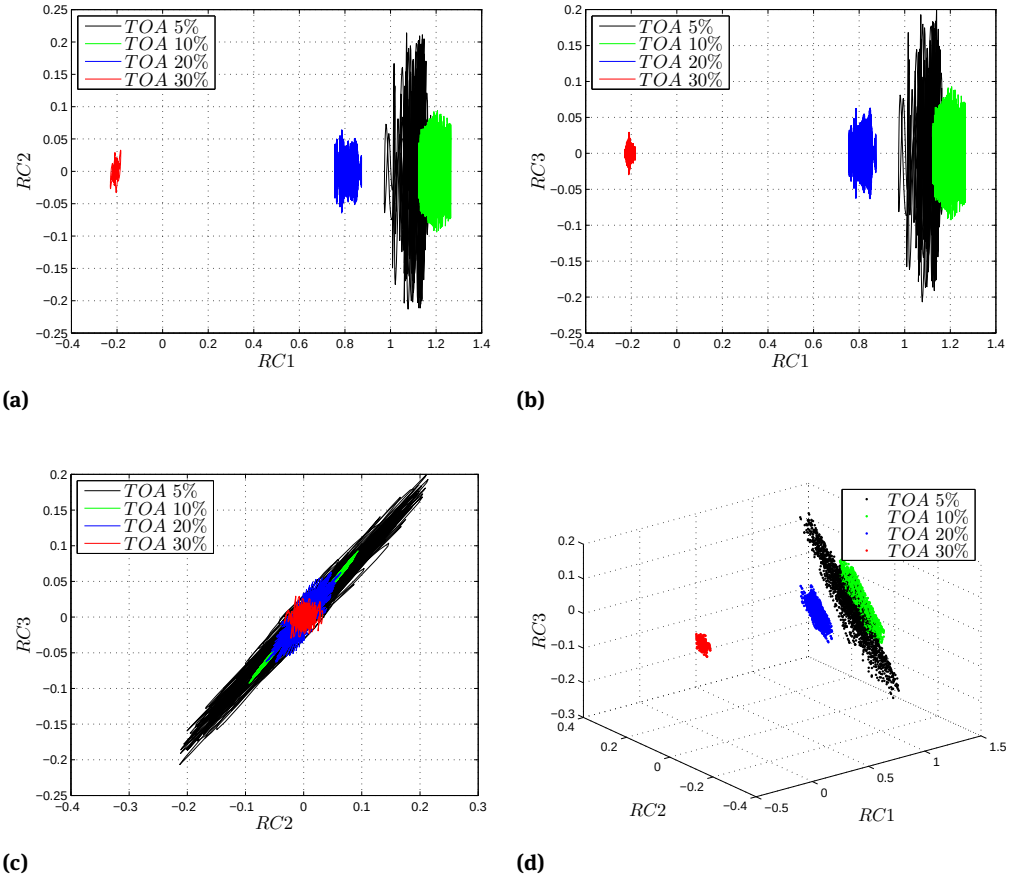

Figure 12: Phase portraits of the blower inlet signal on orthonormal basis created from the first three principal components

of points correspond to $W = 50$.

$$\log\left(\frac{\sigma_i}{\sum_{i=0}^{k}\sigma_i}\right), \quad i = \frac{i}{k} \tag{4}$$

One should note that the normalized singular value in fact corresponds to the logarithm of the immediacy. Hence, difference in singular value by one order of magnitude means that the immediacy of projection of the component onto the signal is 10 times smaller. In all cases the normalized singular value was dropping very quickly, which reflected the small dimension of the problem. In subplot (b) the sum of first three principal components (RC1 + RC2 + RC3) of each signal were compared to the source signal.

3.3 Phase portraits

Figure 12 and 13 presents the phase portrait of time series gathered at the inlet and at the outlet respectively. Each plot contains four signals gathered at the key points selected for the analysis. Time series are presented in 3-dimensional space constructed from three first principal components of the signal: RC1, RC2, RC3. 2-dimensional plots represent projection of the phase portrait onto subspaces constructed from different combinations of two components from RC1, RC2, RC3.

4 Discussion

4.1 Decomposition of signal into principal components

TOA = 30% (design conditions)

Figures 4 and 5 present the decomposition of signals gathered at TOA = 30%. One can observe that at both pressure gauges, the signal was rather flat and PCA resulted in noise reduction. Therefore it is clear that the immediacy of first three components was several orders of magnitude higher than elsewhere. At higher principal components the nor-

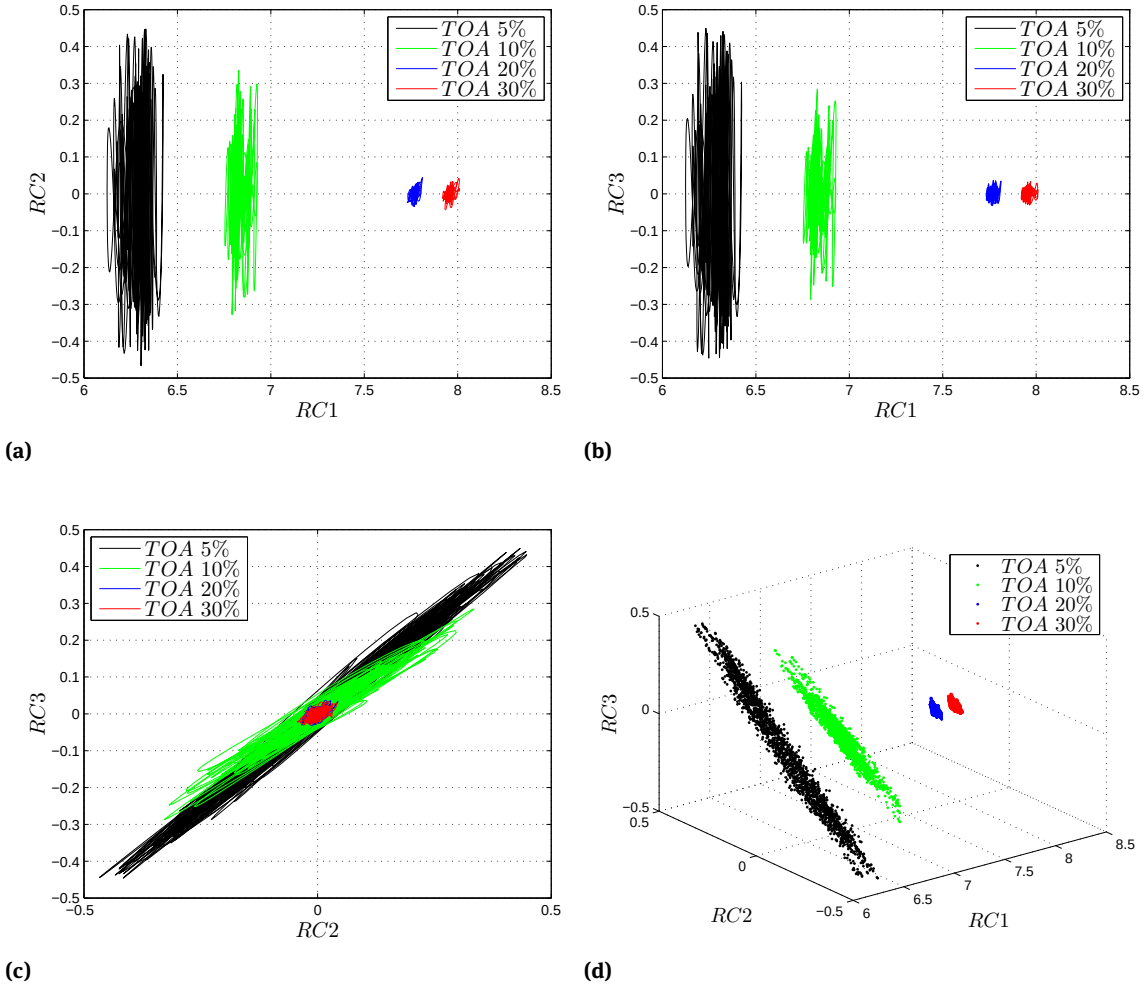

Figure 13: Phase portraits of the blower outlet signal on orthonormal basis created from the first three principal components

malized singular value was contained between −5 and −6 at the inlet. At the outlet it was gradually decreasing to around −12.

TOA = 20% (inlet recirculation)

Kabalyk et al. [26] conducted spectral studies at the same experimental stand. It was shown therein that at TOA = 20% this machine is affected by the inlet recirculation. Indeed, in Figure 6(b) one can observe two features characteristic for this phenomenon: significant rise of the average pressure and random and instantaneous pressure drops. The second feature is not preserved by any of three first principal components. This confirms suspicion raised by Liśkiewicz et al. [14], that these pressure drops have chaotic character. The values of normalized singular value dropped by one order of magnitude at all PC's with exception of the first one, which was still close to one. Figure 7 revealed that the only noticeable change in the outlet pressure signal appeared in its average value, which dropped slightly.

TOA = 10% (pre-surge)

Figure 8 presents pressure time series gathered at the impeller inlet. Pressure drops associated with the inlet recirculation disappeared and were supplemented with much less intensive but regular oscillations. Figure 8(a) shows that higher signal-to-noise ratio resulted in drop of normalized singular value at higher PC's by two orders of magnitude. Figure 9 shows much more noticeable pressure oscillations present in the outlet plenum which is in agreement with the Greitzer theorem of the surge phenomenon [2].

TOA = 5% (deep surge)

TOA = 5% corresponds to the lowest throttle opening area at which the measurements were conducted. At this valve position the machine was undoubtedly at deep surge, which was associated with strong noise and oscillations of the machine. One can observe that both inlet and outlet pressure signal reveals strong recurrent oscillations that are well reproduced by the sum of first three principal components.

4.2 Phase portraits

Inlet

Phase trajectory of signal at stable working conditions (TOA = 30%) has a form of slight oscillations around one point. At the inlet recirculation (TOA = 20%) trajectory oscillates with higher amplitude, especially along RC2 and RC3. This tendency continues and at TOA = 10% and TOA = 5% fluctuations in directions RC2 and RC3 continued to increase. Hence, rise of fluctuations in directions RC2 and RC3 can be associated with unstable machine operation. Projection (c) exhibits that in all cases the phase trajectory (RC2,RC3) oscillates around (0,0). However, the oscillation amplitude increases with decreasing TOA indicating appearance of unstable phenomena. Component RC1 at all TOA oscillates slightly around the value of mean pressure attained at given point.

Outlet

Similarly, the first principal component RC1 of the outlet signal reflects the value of mean pressure. The projection in Figure 13(c) shows that components RC2 and RC3 oscillate around (0,0). In this case the amplitude of oscillation remains very small at TOA = 30% (design conditions) and TOA = 20% (inlet recirculation). This demonstrates clearly that at TOA = 20% the instability appeared in the inlet zone only, while the flow remained stable at the outlet. At TOA = 10% the pre-surge phase oscillations caused noticeable rise in fluctuation of these components, while at the deep surge (TOA = 5%) the fluctuations became stronger.

5 Summary

In the presented study the signals were gathered at inlet and outlet zones of the centrifugal blower and subjected to dynamical study by means of principal component analysis. Signal was decomposed into principal components and then projected onto orthogonal space constructed from the first three components. The main conclusions of this work are listed below:

- Plots of normalized singular values have shown that the system had limited dimension and could be accurately represented with only the first few principal components. In this study, the first three components were analyzed.
- First principal component was reproducing the value of the average pressure. Components number two and three have proven to be of great importance in identification of unstable machine performance.
- At the moment of instability onset the phase portrait transformed into limit cycle with strong oscillations in directions of the second and third principal components.
- Transformation of the phase portrait appeared in any type of instability, including inlet recirculation, which has local character, and deep surge, which has global character.

References

[1] Emmons H.W., Pearson C.E., Grant H.P., Compressor surge and stall propagation. Transactions of ASME, 77(4):455–467, 1955.

[2] Greitzer E.M., Surge and rotating stall in axial flow compressors-part i: Theoretical compression system model. Journal of Engineering for Power, 98(2):190–198, 1976.

[3] Greitzer E.M., Surge and rotating stall in axial flow compressors-part ii: Experimental results and comparison with theory. Journal of Engineering for Power, 98(2):199–211, 1976.

[4] Hansen K.E., Jorgensen P., Larsen P.S., Experimental and theoretical study of surge in a small centrifugal compressor. Journal of Fluids Engineering, 103(3):391–395, 1981.

[5] Moore F.K., Greitzer E.M., A theory of post-stall transients in axial compression systems: Part i-development of equations. Journal of Engineering for Gas Turbines and Power, 108(1):68–76, 1986.

[6] Moore F.K., Greitzer E.M., A theory of post-stall transients in axial compression systems: Part ii-application. Journal of Engineering for Gas Turbines and Power, 108(2):231–239, 1986.

[7] Gravdahl J.T., Egeland O., Speed and surge control for a low order centrifugal compressor model. In Proceedings of the 36th International Conference on Control Applications, San Diego. IEEE. 344–349, 1997.

[8] Ishii H., Kashiwabara Y., Study on surge and rotating stall in axial compressors: A numerical model and parametric study for multiblade-row compressors. JSME International Journal. Series B: Fluids and Thermal Engineering, 39(3):621–631, 1996.
[9] Jansen W., Rotating stall in a radial vaneless diffuser. Journal of Basic Engineering, 86(4):750–758, 1964.
[10] Senoo Y., Ishida M., Kinoshita Y., Asymmetric flow in vaneless diffusers of centrifugal blowers. Journal of Fluids Engineering, 99(1):104–111, 1977.
[11] Abdelhamid A.N., Bertrand J., Distinctions between two types of self excited gas oscillations in vaneless radial diffusers. In Proceedings of Turbo Expo, San Diego, 1979. ASME.
[12] Frigne P., Van den Braembussche R., Distinction between different types of impeller and diffuser rotating stall in a centrifugal compressor with vaneless diffuser. Journal of Engineering for Gas Turbines and Power, 106(2):468–474, 1984.
[13] Lennemann E., Howard J., Unsteady flow phenomena in rotating centrifugal impeller passages. Journal of Engineering for Gas Turbines and Power 92.1 (1970): 65–71.
[14] Liśkiewicz G., Horodko L., Stickland M. et al., Identification of phenomena preceding blower surge by means of pressure spectral maps. Experimental Thermal and Fluid Science, 54:267–278, 2014.
[15] Mizuki S., Kawashima Y., Ariga I., Investigation concerning rotating stall and surge phenomena within centrifugal compressor channels. In Proceedings of International Gas Turbine Conference, London, 1978. ASME.
[16] Packard N.H., Crutcheld J.P., Farmer J.D., et al., Geometry from a time series. Physical Review Letters, 45(9):712, 1980.
[17] Takens F., "Detecting Strange Attractors in Turbulence", Lecture Notes in Mathematics, p.366, Springer, Berlin, 1981.
[18] Palomba C., Breugelmans F., Phase portraits from rotating stall time series, XII ISABE conference, 312–318, Melbourne 1995.
[19] Palomba C., Horst L., Breugelmans F., Strange Attractor Characterization of Rotating Stall in an Axial Flow Compressor. JSME Centennial, 1997.
[20] Hagino N., Uda K., Kashiwabara Y., Prediction and Active Control of Surge Inception of a Centrifugal Compressor. Proceedings of the International Gas Turbine Congress. 2003.
[21] Broomhead D.S., King G., Extracting qualitative dynamics from experimental data. Physica D: Nonlinear Phenomena, 20(2):217–236, 1986.
[22] Komatsubara Y., Mizuki S., Dynamical system analysis of unsteady phenomena in centrifugal compressor. Journal of Thermal Science 6.1 (1997): 14–20.
[23] Gu C., Yamaguchi K., Nagashima T., et al., Observation of centrifugal compressor stall and surge in phase portraits of pressure time traces at impeller and diffuser wall. Journal of fluids engineering 129.6 (2007): 773–779.
[24] Kuzmin V., Khazhuev V., Measurement of liquid or gas flow (flow velocity) using convergent channels with a witoszynski prole. Measurement Techniques, 36(3):288–296, 1993.
[25] Golyandina N., Nekrutkin V., Zhigljavsky A., Analysis of time series structure: SSA and related techniques. CRC Press, 2001.
[26] Jolliffe I., Principal component analysis. Volume 487. Springer-Verlag New York, 1986.
[27] Garcia D., Trendafilova I., A multivariate data analysis approach towards vibration analysis and vibration-based damage assessment. Application for delamination detection in a composite beam. Journal of Sound and Vibration, 333(25), 7036–7050 2014.
[28] Ghil M., Allen M., Dettinger M., et al., Advanced spectral methods for climatic time series, Reviews of Geophysics, 40(1), 3–1 2002.
[29] Kabalyk K., Liśkiewicz G., Horodko L., et al., Use of pressure spectral maps for analysis of influence of the plenum volume on the surge in centrifugal blower. In Proceedings of Turbo Expo, Düsseldorf, 2014. ASME.